

Can viewer proximity be a behavioural marker for Autism Spectrum Disorder?

R. Bishain*, B. Chakrabarti†, J. Dasgupta§, I. Dubey†‡, Sharat Chandran*

[On behalf of the START consortium.]

* Department of Computer Science and Engineering, Indian Institute of Technology Bombay, India

† Centre for Autism, School of Psychology & Clinical Language Sciences, University of Reading, UK

‡ Division of Psychology, De Montfort University, UK

§ Child Development Group, Sangath, Bardez, Goa, India

Abstract—Screening for any of the Autism Spectrum Disorders is a complicated process often involving a hybrid of behavioural observations and questionnaire based tests. Typically carried out in a controlled setting, this process requires trained clinicians or psychiatrists for such assessments. Riding on the wave of technical advancement in mobile platforms, several attempts have been made at incorporating such assessments on mobile and tablet devices.

In this paper we analyse videos generated using one such screening test. This paper reports the first use of the efficacy of using the observer’s distance from the display screen while administering a sensory sensitivity test as a behavioural marker for Autism for children aged 2-7 years. The potential for using a test such as this in casual home settings is promising.

I. INTRODUCTION

Autism Spectrum Disorders (ASD) are associated [1] with atypical social communicative behaviour, restricted range of interests and repetitive behaviour. While the global population-level prevalence of ASD is estimated to be around 1%, the challenges faced in low and middle income countries (LMIC) are significantly greater than those faced by high income countries (HIC) due to the shortage of resources and expertise. Assessment of ASD constitutes the first hurdle in meeting this important global health need.

Patients going to the hospital, even assuming the availability of trained professionals is not scalable. In 2018, Egger *et al.*[2] reported the use of an iPad based method to be used in a home setting in HIC; from the computer vision perspective, the technology of interest was to automatically obtain head pose based on the method in [3] and emotion and attention analysis [4].

These autism screening and diagnostic analyses typically focus on social functioning measures. However, many autistic individuals show an atypical *sensory sensitivity* in one or more modalities [5]. Indeed, recognition of this gap in assessments led to sensory symptoms being included within the diagnostic framework for ASD in the latest version [1] of the diagnostic manual. The sensory sensitivity test in this paper follows ideas similar to [2] but includes the ‘wheel-task’(Sec. I-A) and is administered in LMIC on casual Android platforms.

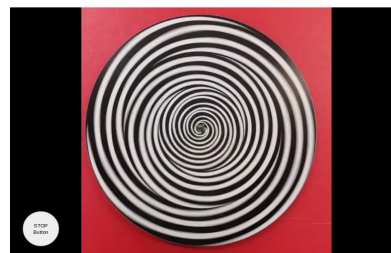
The problem solved in this paper is illustrated in Figure 1 (refer next page). To the best of our knowledge, this is the first evidence of using a computer vision algorithm for the wheel

task for a significant medical condition, with emphasis that the target audience is children in a relaxed LMIC home setting.

A. The wheel task

The objective of the wheel task is to present a ‘rotating’ disk (refer below) on the tablet screen to a child who is being screened for ASD. Autistic children tend to look intently [6] at a spinning wheel as well as come closer to the wheel. While the child is engaged in this task, the front camera of the device records the child’s movement.

In the current work, we investigate the relative movement of the child with respect to the screen. If a child is fascinated by the spinning object they tend to often move closer to the object and thus closer to the front camera. In this paper, we posit that a measure of the relative motion



A spinning wheel is displayed on a tablet screen. Size of the disk as well as the display screen are uniform for all subjects (children)

of the child with respect to the front camera can be used as an indicator of their interest in the spinning object. We then utilise this observation for predicting the diagnostic classification of the child.

Challenges: Although cues such as relative face size can be considered for computing the distance of the child from the screen, we found in our experiments that these proxies for distance are unreliable. The key computational challenge stems from our assumption that different children could be seated at different distances – indeed some children may even run the test in a supine position. Also, the head orientation of a subject can inordinately impact the perceived face size in a two-dimensional image.

It is to be noted that while we administered the tests in an unconstrained home environment, such tests are usually administered in controlled laboratory settings. Also, the tests were conducted by low-skilled health workers in LMIC house-

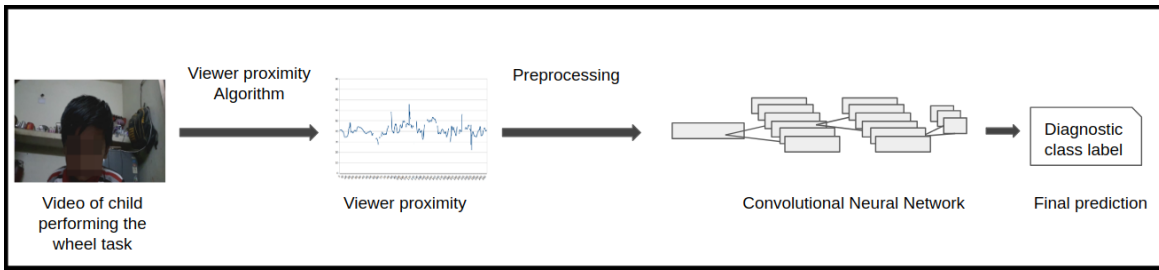


Fig. 1: Overview: The contribution in this paper is to provide (and validate) a method of obtaining viewer distances for children whose pictures are taken in a casual home setup with uncalibrated low resolution cameras and utilise it for diagnostic classification of autism.

holds. The workers were not provided any special training, unlike the clinicians who usually conduct the tests in controlled settings. Hence, our approach addresses this constrained context and aims to capture the viewer’s proximity using images captured from an uncalibrated low resolution camera. Please see the supplementary video on the data capture.

B. Contributions

Tablets recording viewers is becoming increasingly common, to say the least, and face identification is standard. The key technical contributions in this work are

- A method that computes in metric units the distance between the front camera of a tablet and the face of a human being. This measure is often a requirement in such diagnostic analyses. (The source code will be provided)
- A method that works
 - for *children* as they tend to get distracted quickly and may not remain stationary in front of the tablet device during the task.
 - in poorly lit conditions as the study is aimed at children from less privileged backgrounds. (Methods that work in well-lit homes may not generalise across low resolution, poorly lit environments. In this paper, we demonstrate evidence that current computer vision methods are quite robust in home settings.)
- Quantitative evidence that viewer proximity in the wheel task can be a marker for classification in child development. (All earlier work on this task were subjective lab-based assessments. We report the first classifier which utilises this measure for diagnostic classification).

The rest of this paper is organised as follows. We first discuss related work, and follow it up with the method suggested and its validation (Section II). Results are presented in Section III.

C. Related Work

Since ASD is a spectrum of developmental disorders, most of the diagnostic and screening assessments revolve around the analysis of behavioural symptoms. These can be analysed in dyadic interaction between the subject and others. For instance, in the case of young children, by observing

the interaction between mother and child, psychologists can devise an appropriate intervention plan (i.e., therapy) for better parental care and child development.

In such assessments [7] the aim is to capture important behavioural cues such as shared mutual attention, imitating other’s actions, etc. Such play interactions are also analysed for screening and diagnostics [8] purposes and for longitudinal impact assessments [9] of the selected intervention therapy.

Researchers have tried to employ machine vision techniques to automate such analysis but they are either dependent on a multimodal setup or analyse a very structured set of actions under a constrained paradigm. For instance, Rehg *et al.*[10] have analysed behaviour of children by creating an independent Rapid-ABC paradigm. In contrast, Marinoiu *et al.*[11] have attempted both action and emotion recognition tasks in an unstaged environment. However, they have focused on robot assisted therapy and not on the diagnostic aspect of autism which is the focus of our paper.

The analysis of head movement, while children perform autism specific assessments, has gained traction in the computer vision community in recent years. More specifically, Martin *et al.*[12] contrasted head movements between ASD and non ASD groups of children when watching videos of social vs non-social stimuli. They have studied group differences vis-à-vis pitch, yaw and roll of the head movements. Ogiwara *et al.*[13] studied specific temporal patterns of head movements to understand their diagnostic potential.

The studies based on head movement [12] and [13], discussed above, have been carried out in laboratory settings. Children are seated in front of a monitor, with a mounted camera, which records their movement while they view various stimuli on the screen. *In contrast, our work relies solely on videos captured at the home of participant children.* The videos are captured from the relatively weak front camera (0.35 Megapixels) of Android tablet devices while the children view the stimuli presented on the tablet screen.

II. METHODOLOGY

The complete process pipeline, from data capture in the form of videos, to the final diagnostic class prediction, is depicted diagrammatically in Figure 1. The details of each

phase in the process pipeline are elaborated in Sections II-A to II-C.

A. Data Collection

As mentioned, several tasks are administered in determining markers for autism. Typically, the battery of incorporated tasks are carried out in controlled settings in a laboratory with expensive setups, sensors and trackers. In contrast, we are limited in our approach due to the requirements of a low-resource setting. Due to this requirement the data collection was performed using an economical tablet device with additional limitations of:

- No user dependence is permitted (For example, no task or user specific calibration was allowed).
- No separate recording – the recording was only via a low resolution RGB front camera that could be triggered with the task.
- No additional user sensors or wearable setup was allowed.

These limitations are to be contrasted with prior work.

The tasks were conducted by non-specialist community health workers on young children at their homes. This was essential for the desired scalability and for collecting data on autism related symptoms in LMIC. In summary, the task was administered in as natural a setting as possible. In this paper, we have focused only on one of the several tasks which have been incorporated for screening of autism risk.

Diagnostic Category	Video Count	Videos Used
(TD) Typically Developing	39	37
(ASD) Autism Spectrum Disorder	43	41
(ID) Intellectually Disabled	39	37
Total	121	115

TABLE I: Number of wheel task videos collected across the diagnostic categories of TD, ASD and ID children. All data collected on the same device model. Maximum video duration was 80 seconds. As per our knowledge this is the largest dataset for such a task captured in home settings

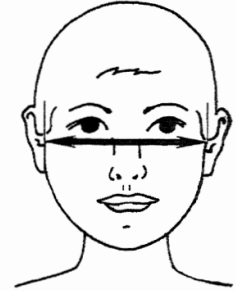
The data is a set of videos of children performing the wheel task. Prior to the data collection the children were categorised in one of the three diagnostic groups by experts in a prestigious medical school-cum-hospital-cum-medical research university that sees a daily footfall of over thousand patients of all ages. In contrast, the video data set is collected by minimally trained workers who have administered these tasks in semi-urban households. A corpus of 121 videos has been created (with 195000 image frames). The videos have been captured across the diagnostic categories or classes of TD (Typically Developing), ASD and ID (Intellectual Disability) children as shown in Table I.

These videos were manually verified for usability in our task and some videos were observed to be unusable due to insufficient length of relevant footage. Finally, after removing such videos a total of 115 videos were used for this analysis with the respective distribution across the three diagnostic classes as shown in Table I. We have included a sample video from this dataset in the supplementary material.

B. Viewer proximity algorithm

As its input, the algorithm receives a video of a user watching a tablet screen as captured from the front camera. The intrinsic (or extrinsic) camera parameters are unknown. As its output the algorithm predicts the user’s distance (in metric units) from the tablet screen in each video frame. There is no expectation that the user will be in a seated position, or in any fixed position. It is conceivable that the user may not be visible while the task is going on since children can be easily distracted.

First we detected the face, and then landmarks within the face using a state-of-the-art deep neural network-based face detector (FAN) [15]. This detector provides, for each frame in the video, a reference 3D value for each landmark in a local coordinate system. However, these 3D coordinates, while valid for each frame, are incomparable across frames. Next, a reference frame is therefore desirable, and we used the frame corresponding to the “most frontal”¹ face amongst all faces in the video.



The length, denoted by the arrowheads, represent the bitrignon breadth ([14], page 188).

The unifying factor across all these frames is, of course, the camera. Since the 2D landmark for each corresponding 3D landmark is available (indeed, that’s how the 3D is estimated in the first place), we were able to use these correspondences to find the camera centre. Once the camera centre is computed, it is relatively straightforward to compute the metric distance to one of the landmarks, such as the left or the right eye. The data from this step is used in ablation Scheme 2 described later.

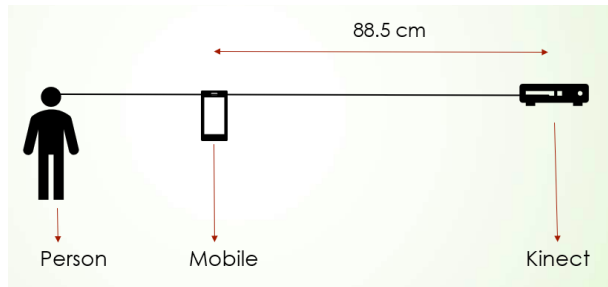
As communicated by domain experts, some child development studies rely on actual Euclidean distance values. Since from a single camera, we cannot obtain Euclidean (metric) values, we use the concept of “bitrignon breadth” – the width between the two trignons (cartilaginous notches at the front of the ear). Once the head pose is calculated in pixel units, we obtain the average depth in real units using the scale factor from the bitrignon breadth of children. The benchmark bitrignon breadth is taken to be 10.6 cm corresponding to the 50th percentile bitrignon breadth for children, both males and females (obtained from [14], page 454). While the head sizes do vary across children, the variation is insignificant in children in our data set who primarily belong in a narrow age range.

1) *Algorithm Correctness*: To validate our approach we need reliable ground truth values for viewer distance from the tablet screen. This ground truth can then be used for validating the results output by our proximity estimation algorithm. We followed two different approaches for validation. The first

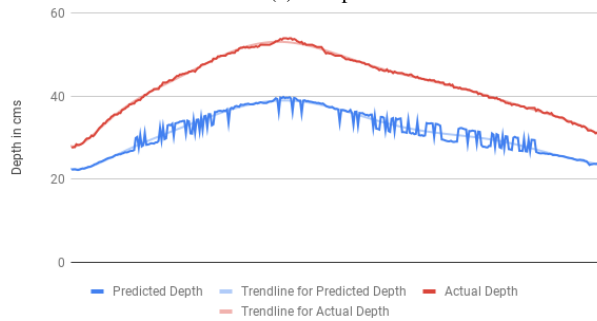
¹Details provided in the supplementary material

approach relied on manually noting the distances for each frame while the second approach relied on a Kinect V2 based annotation setup. Here, we discuss validation using the Kinect device based on the setup shown in Figure 2a (both approaches revealed similar results). In the setup we have placed the tablet device at a distance of 90 cm from the Kinect.

Calibrating Kinect: During the validation process we observed that Kinect prediction in the near camera range was not reliable (During the wheel task children typically tend to watch the screen at a range of 20 – 50 cm from the tablet device. Kinect predictions were first manually verified to be stable and reliable in the 60+ cm range (hence the 90 cm distance mentioned above). More details about Kinect calibration are included in the supplementary material.



(a) Setup



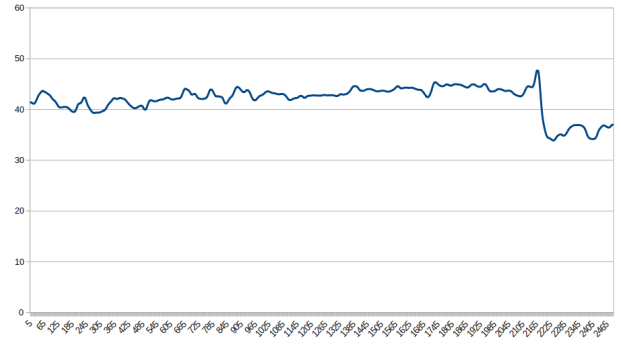
(b) Validation.

Fig. 2: (a) Representative depiction of the Kinect setup to validate the correctness of our algorithm. The actual computation does not use the Kinect. (b) Distance in cm vs the frame number. Our results mimic those of the Kinect. The difference in the estimate in (b) is due to the pixel scaling factor used in our approach which assumes a small child’s head while the validations were performed on adults.

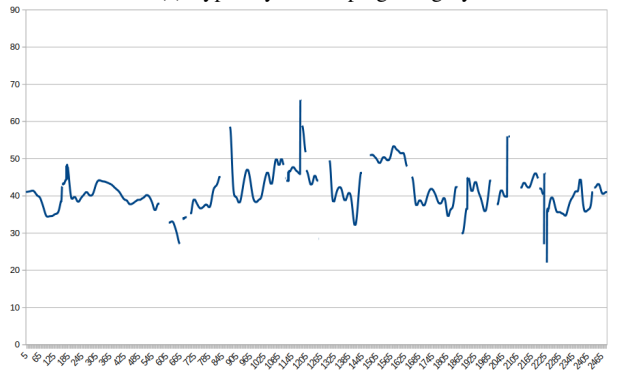
Validating the algorithm: The output of a sample test run on this validation set up is depicted in Figure 2b. In the setup, the viewer is looking at the mobile screen and is initially 30 cm away from it. The viewer moves back up to a distance of 50 cm away from the mobile before returning to the starting point. Note that this translates to a corresponding distance of 118.5 and 138.5 cm in the setup, respectively (refer Figure 2a).

Although they follow the same trend, as shown in Figure 2b, the distance predicted by our approach do not match the

ground truth (values predicted by Kinect). This is expected as the predictions are derived from an assumed bitrignon breadth of 10.6 cm which is typically the value for an average child (the corresponding size for an average adult would be considerably higher). The validation tests were performed by adults). The predicted depth values are filtered (to smoothen out and remove the noise in prediction) before being used for diagnostic classification.



(a) Typically Developing category



(b) Autism Spectrum Disorder category

Fig. 3: Distance in cm vs frame number of the video. These figures show the motion of a child’s head relative to the tablet screen while performing the wheel task from our viewer proximity estimation algorithm.

C. Training

In this section, we describe the process of analysing the viewer movement data in order to predict the diagnostic classification. We utilise the data output by our proximity estimation algorithm as described in Section II-B.

Preprocessing: As is evident from Figure 3a and Figure 3b the movement data is now reduced to a vector containing the estimated distance of the child from the tablet for each frame of the recorded video. The size of the vector depends on how long the task was undertaken (a stop button is provided on the screen for the child). It can range from a few hundred data points to a maximum of 2400 data points (recall that videos in the task are displayed for no more than 80 seconds).

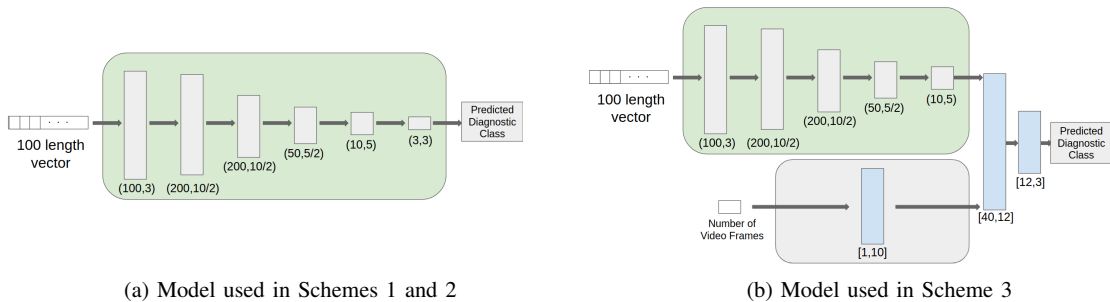


Fig. 4: Network models used across the different schemes. (a) Uses only the fixed length distance vectors as input. Specification provided below each 1D convolution layer as (out channels, kernel size/stride) (b) Additionally uses video duration as an input. Specification of fully connected layers depicted as [in features, out features]. The output from two different channels is concatenated and fed forward to fully connected layers

Since the whole process is natural and free format, there are frames which do not depict the child, i.e., the child has moved out of the screen. These could be a deliberate action on the part of the child (“disinterest”) or could be a momentary glitch (“the tablet is swung out”). One way to handle this is to apply a windowed median filter followed by Gaussian smoothing. Any other kind of preprocessing, e.g. applying transforms, was not considered as the neural network was expected to learn from the raw data.

For larger gaps, there may have been some intent, and we wish to seek to preserve this information. Therefore, if after filtering, the distance estimate is still unavailable, a marker value (‘0’) is substituted with the intention of letting the network learn this event. (Any resulting string of 0s in the vector has been replaced with a single 0 value.) We observed that this replacement stabilised the subsequent learning process.

Since the input vector sizes are of variable length, we extracted contiguous chunks of smaller vectors of size 100 from each input vector. This helped in providing a uniform input size as well as, in essence, boosting the training set size.

The resulting equi-sized vectors are provided as input to a 1D convolutional neural network to predict one of the three diagnostic classes. The network details are shown in Figure 4. Cross entropy loss function was employed to the last layer’s output to arrive at the final predictions. A data split of 7 : 1 : 2 was used for training, validation, and test sets respectively.

Ablation schemes: To further investigate the impact of various factors on the classification accuracy, we have divided the analysis into three broad schemes as described below:

- **Scheme 1:** In this scheme we analyse the movement data as generated by our viewer proximity algorithm (refer Figure 3a). The equi-sized chunks of vectors are input as is to the network model shown in Figure 4a.
- **Scheme 2:** In this scheme we normalise the movement data before providing it as input to the network model as shown in Figure 4a. Since the movement data is estimated based on an average head size (derived using the bitrignon width of an average child), this scheme mitigates any inadvertent impact of this assumption. The movement

data for each child subject is normalised by mean shifting and scaling it down by the respective standard deviation.

- **Scheme 3:** As mentioned earlier the output video duration in our data set differ across child subjects. This duration indicates how long the child was actually engaged in the wheel task. In this scheme we analyse the impact of supplementing the input with video duration (expressed as the number of frames in the video).

To analyse this modified input we have altered our network model. Now, there are two separate inputs provided:

- vector representing the movement data. This part is unaltered and remains consistent with schemes 1 and 2 described above. The output of the penultimate layer is extracted before final inference and concatenated as shown in Figure 4b
- number of video frames for the corresponding video. This input is parsed through a fully connected layer and concatenated with the output of the penultimate layer mentioned above

The concatenated vector is finally parsed through fully connected layers for making the diagnostic classification prediction.

III. RESULTS

A 5-fold cross validation approach was utilised for estimating the network accuracy. Five sets or folds of mutually exclusive data were created with almost equal representation from subjects of each diagnostic class. The selection was randomly performed with no manual considerations. Table II lists the data split for each of the five sets.

Category	Fold1	Fold2	Fold3	Fold4	Fold5
TD	7	8	7	8	7
ASD	8	8	8	8	9
ID	7	8	7	8	7
Total	22	24	22	24	23

TABLE II: Tabular representation of the cross validation process listing the number of children in each diagnostic category.

In each of the five rounds, a different hold out set was chosen from among the five sets. The hold out set was used for testing the model which was trained (and validated) on the remaining 4 sets. Throughout the five rounds a consistent split of 7 : 1 was maintained between the training and validation sets.

Note that a naive classifier, which stubbornly outputs only one class for any subject, would have achieved a maximum classification accuracy of 35.65% (= 41/115). A random scheme would get one out of 3 right (33%).

It is to be noted that the network has been trained for predicting the label for smaller equi-sized input vectors. The final classification for a subject (child) was arrived at by considering the modal value of the predictions for all the constituent smaller vectors for that subject. The resulting prediction accuracies of the models, for the corresponding schemes, have been noted for each of the five rounds as shown in Figure 5. Please note that the average accuracy is arrived at by weighting the round’s accuracy by the size of the corresponding hold out set (i.e., number of subjects in the hold out set).

We observe that Scheme 2 provides better results compared to the other schemes. It can be noted that normalizing the estimated viewer proximity values enhances the overall classification accuracy to 68.69%. Further, we present the confusion matrix for one of the 5 folds of the experiment for Scheme 2. Here, the columns represent the predicted values for a given class. Similar confusion matrices for the remaining folds used for cross-validation have been included in the supplementary material.

Category	TD	ASD	ID
TD	6	2	0
ASD	0	8	0
ID	2	2	4

IV. CONCLUSION

Finding behavioural markers for ASD is a challenging proposition. Nearly all prior work in this direction have only been experimented in a laboratory or a clinic setup. It is desirable if the hospital comes to the child but such a setup poses interesting challenges. This process becomes even more difficult if the hospital comes to the child in the form of a mobile device that has “tasks”.

In this paper, we analysed the “wheel task” in which the front camera of the device is used to record a child watching a “spinning” wheel. To the best of our knowledge, such an analysis has not been performed in the casual setting of a semi-urban home in LMIC countries. We used the viewer proximity as a marker for ASD, and we observed that we could correctly classify a child solely with this measure with an average accuracy of 68.69%. Although this may not seem like a strong result when compared to classification tasks in other domains, it is the first such attempt for this task. Such tasks are usually carried out in lab settings, where the analysis is subjective.

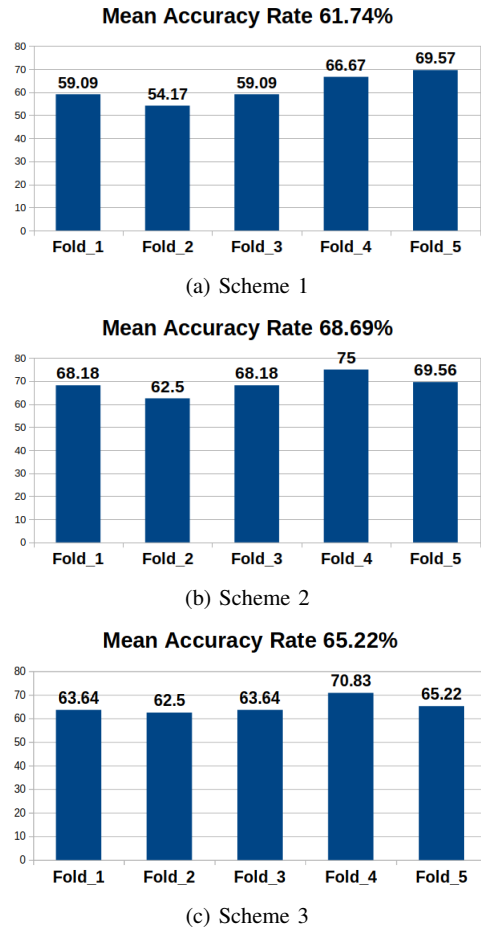


Fig. 5: Accuracy results for the different analysis schemes

Further, our results may be seen as a weak classifier which can assist in such analyses. It is also worth noting that this accuracy is significantly higher than that of a naive classifier. We are able to achieve this through a computer vision algorithm that measures viewer proximity in casual video recordings.

V. ACKNOWLEDGEMENT

The START (Screening Tools for Autism Risk using Technology) consortium members are listed alphabetically: Bhisadev Chakrabarti, Debarati Mukherjee, Gauri Divan, Georgia Lockwood-Estrin, Indu Dubey, Jayashree Dasgupta, Mark Johnson, Matthew Belmonte, Rahul Bishain, Sharat Chandran, Sheffali Gulati, Supriya Bhavnani, Teodora Gliga, Vikram Patel. This work was funded by a Medical Research Council Global Challenge Research Fund grant to the START consortium (PI: Chakrabarti; Grant ID: MR/P023894/1).

REFERENCES

[1] *Diagnostic and statistical manual of mental disorders*, 5th ed., American Psychiatric Association, 2013.

- [2] H. L. Egger, G. Dawson, J. Hashemi, K. L. Carpenter, S. Espinosa, K. Campbell, S. Brotkin, J. Schaich-Borg, Q. Qiu, M. Tepper, J. P. Baker, R. A. Bloomfield, and G. Sapiro, "Automatic emotion and attention analysis of young children at home: a ResearchKit autism feasibility study," *NPJ Digital Medicine*, vol. 1, no. 1, pp. 1–10, 2018.
- [3] X. Xiong and F. De la Torre, "Supervised descent method and its applications to face alignment," in *CVPR*, 2013, pp. 532–539.
- [4] J. Hashemi, K. Campbell, K. L. Carpenter, A. Harris, Q. Qui, M. Tepper, S. Espinosa, B. J. S., S. Marsan, R. Calderbank, J. Baker, H. L. Egger, G. Dawson, and G. Sapiro, "A scalable app for measuring autism risk behaviours in young children," in *MOBIHEALTH*, 2015.
- [5] S. Baron-Cohen, E. Ashwin, C. Ashwin, T. Tavassoli, and B. Chakrabarti, "Talent in autism: hyper-systemizing, hyper-attention to detail and sensory hypersensitivity," *Philosophical Transactions of the Royal Society B: Biological Sciences*, vol. 364, no. 1522, pp. 1377–1383, 2009.
- [6] T. Tavassoli, K. Bellesheim, P. M. Siper, A. T. Wang, D. Halpern, M. Gorenstein, and J. D. Buxbaum, "Measuring sensory reactivity in autism spectrum disorder: application and simplification of a clinician-administered sensory observation scale." *Journal of Autism and Developmental Disorders*, vol. 46, no. 1, pp. 287–293, 2016.
- [7] S. Freeman and C. Kasari, "Parent–child interactions in autism: Characteristics of play," *Autism*, vol. 17, no. 2, pp. 147–161, 2013.
- [8] J. M. Guercio and A. D. Hahs, "Applied behavior analysis and the autism diagnostic observation schedule (ADOS): A symbiotic relationship for advancements in services for individuals with autism spectrum disorders (ASDs)," *Behavior analysis in practice*, vol. 8, no. 1, pp. 62–65, 2015.
- [9] A. Pickles, A. Le Couteur, K. Leadbitter, E. Salomone, R. Cole-Fletcher, H. Tobin, I. Gammner, J. Lowry, G. Vamvakas, S. Byford, and C. Alfred, "Parent-mediated social communication therapy for young children with autism (PACT): long-term follow-up of a randomised controlled trial," *The Lancet*, vol. 388, no. 10059, pp. 2501–2509, 2016.
- [10] J. Rehg, G. Abowd, A. Rozga, M. Romero, M. Clements, S. Sclaroff, I. Essa, O. Ousley, Y. Li, C. Kim, and H. Rao, "Decoding children's social behavior," in *CVPR*, 2013, pp. 3414–3421.
- [11] E. Marinou, M. Zanfir, V. Olaru, and C. Sminchisescu, "3D human sensing, action and emotion recognition in robot assisted therapy of children with autism," in *CVPR*, 2018, pp. 2158–2167.
- [12] K. B. Martin, Z. Hammal, G. Ren, J. F. Cohn, J. Cassell, M. Ogihara, J. C. Britton, A. Gutierrez, and D. S. Messinger, "Objective measurement of head movement differences in children with and without autism spectrum disorder," *Molecular Autism*, vol. 9, no. 1, p. 14, 2018.
- [13] M. Ogihara, Z. Hammal, K. B. Martin, J. F. Cohn, J. Cassell, G. Ren, and D. S. Messinger, "Categorical timeline allocation and alignment for diagnostic head movement tracking feature analysis," in *CVPR Workshops*, 2019, pp. 43–51.
- [14] R. G. Snyder, L. W. Schneider, L. O. Clyde, M. R. Herbert, D. H. Golomb, and M. A. Schork, "Anthropometry of infants, children, and youths to age 18 for product safety design. final report." 1977, last accessed: Apr 2020. [Online]. Available: <https://math.nist.gov/~SResler/anthrokids/child77lnk.pdf>
- [15] A. Bulat and G. Tzimiropoulos, "How far are we from solving the 2D & 3D face alignment problem?(and a dataset of 230,000 3D facial landmarks)," in *ICCV*, 2017, pp. 1021–1030.

I. SUPPLEMENTARY MATERIAL

A. Sample Videos

Please refer to the attached video files for a demonstration

1) *Sample wheel task video*: This attached video provides an example of the video of a child performing the wheel test in a home setting. Please note that the video has been modified to protect the privacy of the participant. (For instance, the yellow box is added to detect and subsequently blur the child's face).

2) *START A field data collection app for autism screening*: The wheel test is one of several assessments which are used for screening. We collected data on various other tests by taking a tablet directly to households. Like the wheel test, these assessments too are part of an app which is installed on

the tablet. For context, we provide this attached video

B. Kinect Calibration

Kinect depth prediction values were not in centimeter units. We have arrived at the correlation between the Kinect predicted depth values to the actual distance in cm, as shown in Figure 1. To arrive at this relation both the Kinect device and a plane object were kept on a level surface. The object was then kept at various distances in the 90-120 cm range from the Kinect. The predicted Kinect depth is plotted against the actual object distance to arrive at the approximation given by the following formula $y = 1.91x + 581$, where y is the depth of the object as predicted by Kinect, and x is the ground truth observed distance of the object.

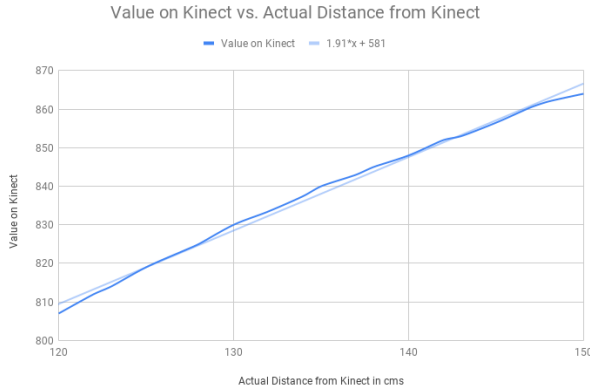
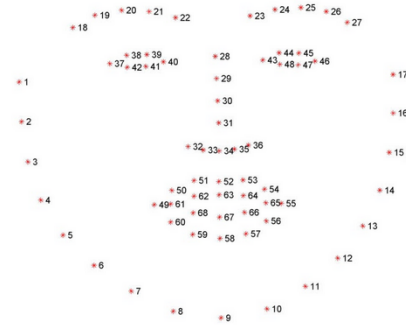


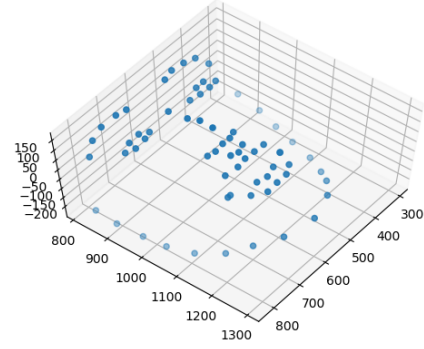
Fig. 1: Correlation between Kinect predicted depth values and the actual distance in cm. The Y-axis represents the depth value as predicted by Kinect. The corresponding ground truth observed distance is plotted on the X-axis. This correlation is used to convert the Kinect predictions to the actual distance in centimetres.

C. Deriving most frontal face

In this section we provide the steps to determine the frame with the most 'frontal' face in a video. The intention is to



(a) 2D facial landmarks



(b) 3D facial landmarks

Fig. 2: Plots of (a) 2D and (b) 3D facial landmarks used to arrive at the most frontal face

capture the image frame in which the user's face tends to be most upright and parallel to the image plane.

The following steps are performed for arriving at the most frontal face:

Input: 68 facial landmarks as shown in Figure 2 for each frame

Output: Frame number with the most frontal face

Calculation steps:

- 1) For each image frame in the video:
 - a) Mean shift the landmarks (using mean of the landmarks in the current frame)
 - b) Scale each landmark down by its corresponding magnitude
 - c) Obtain the (absolute) depth difference for opposite landmark point pairs on the jaw-line (landmark point pairs – 1:17, 2:16, 3:15, ...8:10). Select the maximum 'depth difference' for this image frame from these values
- 2) From among the frames having ± 4 degree 'eyeline orientation', select the $\min(\max(\text{depth difference}))$. i.e. Note the frame with with minimum of the maximum depth difference calculated in step 1c above. For calculation of 'eyeline orientation' the steps are:

- a) Obtain centroid of eyes (centroid of landmark points 37-42 and 43-48)
- b) Obtain eyeline orientation as the slope of the line joining the two eye centroids

D. Confusion Matrices

We present the confusion matrix for each of the five folds below (see main paper for description) for Scheme 2 here. Note that the precision and recall value for each fold is indicated in the last row and column, respectively of the corresponding fold. As before, columns represent the predicted values for a given class.

The overall precision and recall values have been depicted in Table VI

Category	TD	ASD	ID	Recall
TD	5	0	2	0.71
ASD	0	7	2	0.78
ID	0	3	4	0.57
Precision	1	0.7	0.5	

TABLE I: Fold 1 confusion matrix

Category	TD	ASD	ID	Recall
TD	6	2	0	0.75
ASD	0	8	0	1
ID	2	2	4	0.5
Precision	0.75	0.67	1	

TABLE II: Fold 2 confusion matrix

Category	TD	ASD	ID	Recall
TD	5	1	1	0.71
ASD	3	5	0	0.63
ID	1	1	5	0.71
Precision	0.56	0.71	0.83	

TABLE III: Fold 3 confusion matrix

Category	TD	ASD	ID	Recall
TD	4	2	2	0.5
ASD	0	7	1	0.88
ID	0	4	4	0.5
Precision	1	0.54	0.57	

TABLE IV: Fold 4 confusion matrix

Category	TD	ASD	ID	Recall
TD	6	1	0	0.86
ASD	0	7	1	0.88
ID	1	4	2	0.29
Precision	0.86	0.58	0.67	

TABLE V: Fold 5 confusion matrix

Category	TD	ASD	ID	Average Recall
TD	26	6	5	0.7
ASD	3	34	4	0.83
ID	4	14	19	0.51
Average Precision	0.79	0.63	0.68	

TABLE VI: Overall Precision and Recall

E. Mean reciprocal rank (MRR)

We report an average MRR of 0.83 for the five folds for Scheme 2. The MRR values for individual folds are as shown below in Table VII

Fold No.	1	2	3	4	5	Overall
MRR	0.826	0.792	0.818	0.854	0.833	0.825

TABLE VII: Mean Reciprocal Rank for Scheme 2